

This is a postprint version of the following published document:

Marugán-Cruz, C., Serrano, D., Gómez-Hernández, J. & Sánchez-Delgado, S. (2019). Solar multiple optimization of a DSG linear Fresnel power plant. *Energy Conversion and Management*, vol. 184, pp. 571–580.

DOI: [10.1016/j.enconman.2019.01.054](https://doi.org/10.1016/j.enconman.2019.01.054)

© 2019 Elsevier Ltd.



This work is licensed under a [Creative Commons Attribution-NonCommercial-NoDerivatives 4.0 International License](https://creativecommons.org/licenses/by-nc-nd/4.0/).

# Solar multiple optimization of a DSG Linear Fresnel power plant

Carolina Marugán-Cruz<sup>a,\*</sup>, D. Serrano<sup>a</sup>, J. Gómez-Hernández<sup>a</sup>, S. Sánchez-Delgado<sup>a</sup>

<sup>a</sup>*Energy System Engineering Group (ISE). Department of Thermal and Fluids Engineering. Universidad Carlos III de Madrid, Spain*

---

## Abstract

Linear Fresnel power plants are currently one of the most promising concentrating solar power plants, however there are only a few commercial projects. These power plants have lower efficiency than parabolic trough collectors plants and are still expensive. To increase the efficiency of these plants the utilization of water/steam in the receivers (direct steam generation, DSG) and thermal storage (TES) has been considered.

As case-study, a 50 MW<sub>e</sub> solar-only linear Fresnel power plant located at Seville, Spain has been considered. The effects of the solar field size as well as, the thermal storage size, on the annual production of the plant have been analyzed: Nine different solar field sizes and up to eight thermal storage sizes have been compared.

An economic optimization is presented in order to determine which plant has lowest Levelized Cost of Electricity (LCOE). **It has been found that for the power plants with no-storage the optimum solar multiple (SM)**

---

\*Corresponding author

*Email address:* cmarugan@ing.uc3m.es (Carolina Marugán-Cruz)

is 1.7, whereas for the cases with thermal storage, the optimum configuration is a larger solar field (SM= 2), with a thermal storage of 2 hours.

*Keywords:* Solar multiple, Lineal Fresnel, Thermal Storage, Levelized Cost of Electricity

---

## **Nomenclature**

### *Abbreviations*

CSP: Concentrated Solar Power

CRF: Capital recovery Factor (-)

DNI: Direct normal irradiance ( $W/m^2$ )

DSG: Direct Steam Generation

IAM: Incidence Angle Modifier

IRR: Internal Rate of Return

LCOE: Levelized Cost of Electricity [ $c\text{€}/kWh_e$ ]

LFR: Linear Fresnel Reflector

PCM: Phase Change Materials

PTC: Parabolic Trough Collector

TNPV: Total Net Present Value

SM: Solar Multiple

SPT: Solar Power Tower

TES: Thermal Energy Storage

### *Symbols*

$A$ : Area [ $m^2$ ]

$A_p$ : Aperture area [ $m^2$ ]

$B_k$ : Annual revenue [€]  
 $C_{invest}$ : Investment cost [€/kW<sub>e</sub>]  
 $C_k$ : Annual expenses [€]  
 $C_{O\&M}$ : Operation and maintenance costs [€/kW<sub>e</sub>]  
 $E_{ann}$ : Annual energy yield [GWh]  
 $f_{ins,ann}$ : Annual insurance cost [%]  
 $H_{rc}$ : Receiver height above primary reflector [m]  
IC: Investment costs [€]  
 $i_{rate}$ : Debt interest rate [%]  
 $K$ : Correction factor  
 $L$ : Length [m]  
 $\dot{m}$ : mass flow rate of steam [kg/s]  
 $n$ : Service period [years]  
 $N$ : Number  
 $P$ : Pressure [Pa]  
 $q_{pipes}$ : Piping thermal losses [W/m<sup>2</sup>]  
 $\dot{Q}$ : Thermal power [kW<sub>t</sub>h]  
 $r$ : Interest rate of the loans [%]  
 $RY$ : Repayment period [year]  
ST: Local Solar Time [h]  
 $T$ : Temperature [°C]  
 $\dot{W}$ : Power of the cycle [MW<sub>e</sub>]

*Greek letters*

$\alpha$ : Solar altitude angle [rad]

$\gamma$ : Solar azimuth angle [rad]

$\eta$ : efficiency

$\theta$ : Incident angle [rad]

$\tau$ : Discount rate [%]

### *Subindex*

amb: ambient

ave: average cu: control unit

e-m: electro-mechanical

end: end losses

inc: incident

l: longitudinal

loop: collector loops or rows

mir: mirrors

PB: power block

off: off-design conditions

ref: reference conditions

SF: solar field

shad: shaded

T: turbine

Tot: total solar field

t: traverse

O: optical

## 1. Introduction

Reducing the green gas emissions comes along with reducing the dependence on fossil fuels and the deployment of renewable energies, but new technologies must compete on cost with the more classic energy sources. Concentrated solar technology can be used to generate electricity either: by using solar energy as the only resource to power a Rankine cycle (Mills, 2004) or by hybridating solar energy with conventional power-plants (Yang et al. (2011); Li et al. (2017); Petrakopoulou et al. (2017)). Alternative uses of concentrated solar energy are heat supply for different industrial sectors (Farjana et al. (2018)) or covering refrigeration demands (Al-Alili et al. (2012)). Concentrating solar power (CSP) is an important alternative for providing clean and secure energy.

Currently there are four main technologies in CSP: solar power towers (SPT), dish Stirling, parabolic trough collectors (PTC) and linear Fresnel reflectors (LFR). Solar power towers and dish Stirling are point focus techniques while parabolic troughs and Fresnel collectors are known as line focus technologies. Among CSP techniques, parabolic trough collectors have been commercially proven more than any other, however linear Fresnel collectors are significantly less expensive and can be an alternative to PTC.

Linear Fresnel technology is composed of many long flat, or slightly curved, reflectors which focus on an elevated receiver parallel to the reflectors axis (Mills and Morrison (2000)). The receiver is typically mounted on a structure suspended above the mirror arrays (at 5 -15 m high) which does not need to be supported by the tracking device (Desai and Bandy-

26 opadhyay (2017)). The LFR technology is significantly cheaper than the  
27 parabolic trough (Barlev et al. (2011)), mainly due to the cheaper mirrors  
28 and lower structural costs. There are other important advantages such as  
29 low wind loads or lower maintenance costs that could turn this technol-  
30 ogy an alternative to parabolic troughs, despite their much lower overall  
31 efficiency (Kumar and Reddy, 2012; Morin et al., 2012).

32 The design of the LFR can be tailored to use in different applications de-  
33 pending on the temperature of the heat generation (Zhu et al. (2014)). High  
34 temperature heat is generally used to generate electricity (Mills (2004);  
35 Desai and Bandyopadhyay (2017)), whereas low - or - medium temper-  
36 ature heat LFR technology has been used for multiple purposes such as:  
37 building cooling (Velázquez et al. (2010); Mokhtar et al. (2010)) and heat-  
38 ing (Mokhtar et al. (2016)), industrial process heat supply (Mokhtar et al.  
39 (2015); Pulido-Iparraguirre et al. (2019)), or post-combustion carbon-capture  
40 (Wang et al. (2017)).

41 Typically the fluid heated in the LFR receiver is high-pressure water  
42 (Desai and Bandyopadhyay (2017)) that can be used directly in the steam  
43 turbine in a Rankine cycle. The obvious advantage of direct steam gen-  
44 eration (DSG) power plants is that heat exchangers are not necessary and  
45 that the energy efficiency can be higher. Recent studies have evaluated the  
46 performance of the LFR using other fluids such as molten salts (Schenk  
47 et al. (2014); Grena and Tarquini (2011); Qiu et al. (2015); Bacheller and  
48 Stieglitz (2017)), or thermal oil (Cau and D. (2014); Wang et al. (2017)).  
49 Despite the advantages of using those fluids, all commercial LFR power  
50 plants currently in operation and under development or construction use

51 water/steam as working fluid.

52 The SunShot Initiative, that funds programs for concentrating solar  
53 power deployment, has as a goal to lower the cost of CSP to 0.06\$ per  
54 kWh by 2020. Since the solar field represents the major investment in these  
55 power plants (Kolb et al. (2011); Desai and Bandyopadhyay (2017) ) the  
56 optimization of the size of the solar field is critical to reduce the costs of  
57 electricity. Thermal energy storage (TES) and operation strategy are other  
58 factors that affect importantly the price of electricity. Indeed, thermal stor-  
59 age allows to decouple the solar radiation from the electrical output and  
60 thereby can generate electricity during peak hours (Guédez et al., 2016).  
61 This dispatchability has to be taken into consideration when analyzing  
62 the viability of the solar projects (Kost et al., 2013)

63 To this regard, Izquierdo et al. (2010) studied the effects of the solar  
64 field size, the capacity factor and the storage capacity on the cost of elec-  
65 tricity in parabolic troughs and molten salts tower plants. For both tech-  
66 nologies, they noted that for each storage capacity, as the solar field in-  
67 creased, there was an initial reduction in the energy cost up to a minimum.  
68 Luo et al. (2017) studied the optimum solar field size for a steam genera-  
69 tion dual-receiver solar tower with storage. They concluded that the so-  
70 lar field size was the sub-system that affected mostly the LCOE. Montes  
71 et al. (2009b) studied the influence of the solar field size on the annual per-  
72 formance of the power plant of a solar-only thermal-oil parabolic trough  
73 collector plant. Montes et al. (2009a) described the role of the solar field  
74 size on the performance of a hybrid (fossil-solar) DSG PTC power plant  
75 with thermal storage. Giostri et al. (2012) compared the effects of differ-



76 ent heat transfer fluids (molten salt, synthetic oils and water/steam) in  
77 parabolic plants with no thermal storage, and concluded that DSG plants  
78 have higher on-design and annual average efficiency than using any other  
79 fluid. Similarly, Feldhoff et al. (2012) compared the use of DSG and oil  
80 in parabolic plants with integrated thermal storage. Morin et al. (2012)  
81 presented the costs that DSG linear Fresnel technology should have in or-  
82 der to be competitive with DSG Parabolic Troughs. Schenk et al. (2014)  
83 performed an energetic and economical comparison between a parabolic  
84 trough and linear Fresnel collector power plant with Solar Salt as heat  
85 transfer fluid.

86 Although TES technology for DSG is still immature and expensive (Feld-  
87 hoff et al., 2012), significant efforts have been made for its development.  
88 Steam accumulators have been integrated with DSG tower power plants to  
89 provide energy storage for: PS10 (11 MW<sub>e</sub> - 1 h of TES), PS20 (20 MW<sub>e</sub> - 1  
90 h of TES) and Khi Solar One (50 MW<sub>e</sub> - 2 h of TES) (González-Roubaud  
91 et al., 2017). However, this TES technology, which is relatively simple  
92 and mature, presents the drawbacks of the high volume needed to store  
93 large energy quantities and the low storage temperature. Furthermore,  
94 it presents higher costs compared to molten salt TES systems for energy  
95 storages longer than 1 h (González-Roubaud et al., 2017).

96 The results showed the feasibility of the PCM unit for working in con-  
97 stant and sliding pressure modes (Laing et al., 2013). The low thermal con-  
98 ductivity of the PCM, which leads to slow charging and discharging rates,  
99 could be solved installing fins (Laing et al., 2012) or combining the PCM  
100 with an additive of high conductivity, such as graphite (Gil et al., 2010). In

101 this sense, a parametric study determined the target costs of a finned PCM  
102 tank coupled to a DSG PTC power plant (Seitz et al., 2017). The PCM fea-  
103 sibility has been also studied in a cogeneration plant (Saarland, Germany),  
104 storing 1.5 MWh at a power level of about 6 MWth (Johnson et al., 2015,  
105 2017). Other TES configurations for a DSG power plant of 147 MW<sub>e</sub> com-  
106 bine molten salt and PCM to provide different TES capacities (Prieto et al.,  
107 2018).

108 More recently, (Guo et al., 2018) studied different tank configurations  
109 using liquid lead-bismuth eutectic alloy as sensible heat storage and sodium  
110 nitrate as latent heat storage. A three-tank latent heat storage system  
111 showed the highest flexibility of the TES configurations considered for a  
112 DSG PTC.

113 Presently, the DSG linear Fresnel plants of Zhangjiakou and Zhangbei  
114 (under development) use solid state formulated concrete units for storage  
115 (NREL, 2018).

116 Bellos et al. (2018) studied the daily performance of a LFR collector but  
117 to the best of our knowledge, this is the first study to present an economic  
118 optimization of the solar multiple and the thermal energy storage size for  
119 a DSG linear Fresnel power plant.

120 The present paper compares the annual behavior of linear Fresnel power  
121 plants with different solar field sizes and different storage capacity. A 50  
122 MW<sub>e</sub> linear Fresnel power plant with no thermal storage has been chosen  
123 as a reference case. The paper is structured as follows: in section 2, a de-  
124 scription of the components and parameters of the solar power plant is  
125 presented, in section 3 the different solar field sizes and storage capacities

126 are proposed and in section 4 the annual performance of the plant is pre-  
127 sented together with an economical analysis. Finally the conclusions are  
128 discussed in the last section of the manuscript (section 5).

## 129 **2. Solar Power Plant Description**

130 The typical size of a solar power plant is 50 MW<sub>e</sub> or smaller (NREL,  
131 2018) and hence, the power block considered here is a 50 MW<sub>e</sub> reheat re-  
132 generative Rankine cycle. Steam turbines used for CSP applications typi-  
133 cally consist of a high pressure turbine and an intermediate / low-pressure  
134 turbine, with several extractions to preheat the steam. To prevent a large  
135 humidity fraction at the exit of the steam turbine, reheating is necessary.

136 A scheme of the power plant can be seen in figure 1. As was said above,  
137 two cases have been considered: with no thermal storage and with ther-  
138 mal storage. In the first case, when the solar thermal field is generating  
139 enough thermal energy the power block will be able to work at nominal  
140 conditions, at full load, or otherwise the power block will work at part-  
141 load conditions. If the solar power plant has thermal storage, the power  
142 block will be able to operate for longer periods and it is decoupled from  
143 the thermal energy production. The details of the operation when storage  
144 is considered are explained bellow (see 2.3).

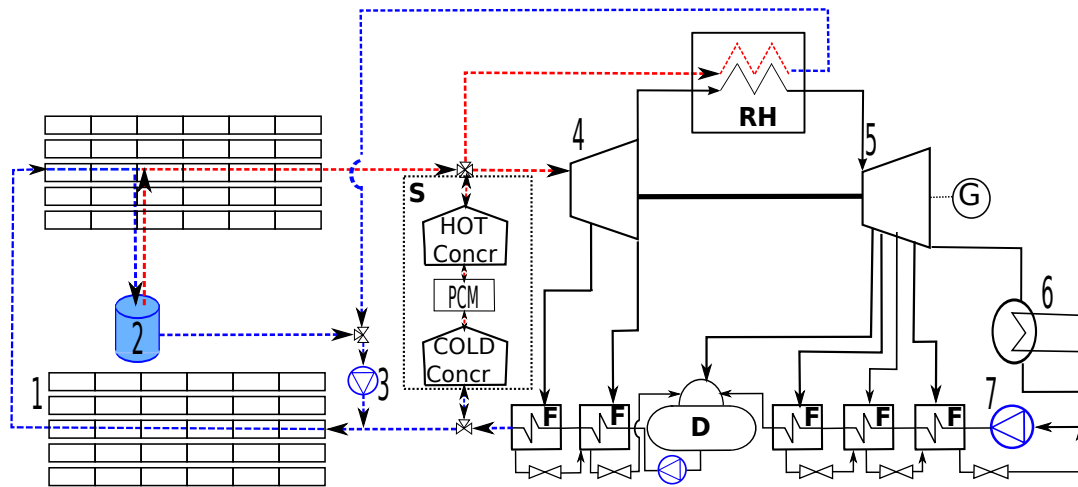


Figure 1: Simplified scheme of the linear Fresnel solar field and power plant: 1. Fresnel solar field. 2. Steam separator. 3. Recirculating solar field pump. 4. High Pressure Turbine. 5. Low Pressure Turbine. 6. Condenser. 7. Condenser pump. **RH**. Reheater. **F**. Feedwater heater. **D**. Deaerator. **S**. Storage system. **G**. Generator

145 *2.1. Fresnel plant configuration*

146 The main components of the Fresnel collectors are the primary mirrors  
 147 that are supported by the tracking structure, the receiver, that typically  
 148 consists of a vacuum absorber tube and secondary reflector, the control  
 149 system for the primary reflectors tracking the sun and the foundation (see  
 150 figure 2). Other designs have been proposed and are under the conceptual  
 151 design stage or might have undergone the prototype phase (Abbas et al.  
 152 (2012); Singh et al. (2010); Zhu et al. (2014)).

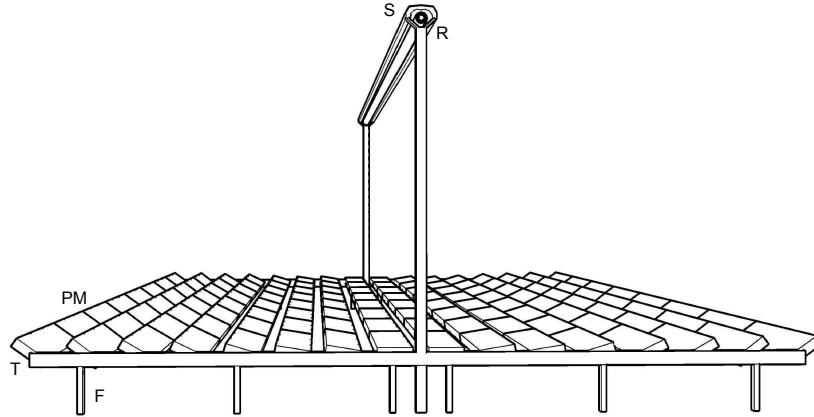


Figure 2: Control unit of a linear Fresnel Collector: F: Foundation, T: Tracking Structure, PM: Primary mirrors, S: Secondary Reflector, R: Receiver tube.

153 There are few linear Fresnel collectors currently being setup commer-  
 154 cially for power production: NOVA-1, SUPERNOVA and DMS of Novatec  
 155 Solar company (Novatec Solar, 2017), Industrial Solar LF-11 (Industrial So-  
 156 lar, 2017) or SUNCNIM (SUNCNIM, 2017). For the following study the  
 157 SUPERNOVA system by Novatec Solar company has been used. This sys-  
 158 tem can achieve steam temperatures up to 550 °C (Novatec Solar, 2017).

159 The smallest unit of the SUPERNOVA system is called control unit (see  
 160 figure 2). Each control unit consists of 16 parallel rows of flat glass mir-  
 161 rors and each row is composed of 8 mirrors, arranged longitudinally. The  
 162 parallel primary mirrors (individually tracked) focus the direct solar ra-  
 163 diation onto the receiver located on top. The control units are arranged  
 164 longitudinally to form a collector row (or loop), and each collector row  
 165 has between 5 or 22 control units. The collector rows can be arranged in  
 166 parallel to form a solar field. A distance of 4.5 m between each collector

167 row is recommended. Table 1 shows the geometrical and optical parame-  
 168 ters of these solar collectors.

Parameter	Value
Number of rows of mirrors per control unit	16
Number of primary mirrors per row	8
Primary mirrors width (m)	0.75
Primary mirrors length, $L_{mir}$ (m)	5.35
Distance between mirrors in a row (m)	0.2857
Distance between rows in a control unit (m)	0.304
Aperture surface of the control unit, $Ap_{cu}$ (m <sup>2</sup> )	513.6
Control unit length, $L_{cu}$ (m)	44.8
Control unit width (m)	16.56
Number of control units per collector row, $N_{cu}$	16
Clearance between collector rows (m)	4.5
—	—
Receiver type	Schott PTR 70
Receiver height above primary reflectors, $H_{rc}$ (m)	7.4
Absorber outer diameter (m)	0.07
Absorber inner diameter (m)	0.065
Glass envelope outer diameter (m)	0.115
Glass envelope inner diameter (m)	0.109
Optical efficiency, $\eta_0$	0.64

Table 1: Geometrical and optical parameter of the Fresnel collectors (Lovegrove and Stein (2012); Novatec Solar (2017); Schott (2017)).

169 The total aperture area of the solar field,  $A_{SF}$  is calculated as:

$$170 \quad A_{SF} = N_{loop} \cdot A_{loop} = N_{loop} \cdot N_{cu} \cdot A_{p_{cu}} \quad (1)$$

171 where  $N_{loop}$  is the total number of collector rows in the solar field and  $A_{loop}$   
172 is the area of the collector row.

173 The solar field design chosen for this study is a recirculating field with  
174 superheating: an evaporator section and a super-heater section separated  
175 by a water-steam separator. One-through steam flow would also be possi-  
176 ble but it is more complex to control (Wagner and Zhu, 2012).

## 177 2.2. Power block

178 An schematic diagram of the steam cycle is shown in figure 1. It is a re-  
179 generative Rankine cycle. Live steam pressure and temperature are chosen  
180 to be 500 °C and 112 bar (Feldhoff et al. (2012, 2010)). In the same figure it  
181 can be seen that reheating is performed between the high and low pressure  
182 turbines to reduce the humidity at the exit, so low pressure turbine inlet  
183 temperature is set to 500 °C at nominal conditions. Six regenerative water  
184 heaters are employed: two extractions from the high pressure turbine and  
185 four extractions from the low pressure turbine.

186 The thermal efficiency of the power block at full load (nominal condi-  
187 tions) is  $\eta_{T,ref} = 42.41\%$  and the electro-mechanical efficiency of the gener-  
188 ator,  $\eta_{e,m}$  is 98.0%. The nominal values of the Rankine cycle are shown in  
189 table 2.

<b>PARAMETER</b>	<b>VALUE</b>
<b>Turbine</b>	
Inlet temperature (°C)	500
Inlet pressure (bar)	112
High pressure efficiency (%)	84
Reheat inlet temperature (°C)	500
Low pressure efficiency (%)	92
Electro-mechanical efficiency (%)	98
<b>Extraction point pressures</b>	
Extraction 1 (bar)	40.0
Extraction 2 (bar)	15.3
Extraction 3 (deaerator) (bar)	8.0
Extraction 4 (bar)	3.4
Extraction 5 (bar)	1.2
Extraction 6 (bar)	0.35
<b>Pressure drop in extraction and reheating</b>	
Extraction line 1 (%)	2.5
Extraction line 2 (%)	3
Reheating line (%)	11.75
Extraction line 3 (deaerator) (bar)	4.5
Extraction line 4 (%)	3
Extraction line 5 (%)	3
Extraction line 6 (%)	3.50
<b>Closed feedwater heaters</b>	
Terminal temperature difference (°C)	1.5
Drain cooling approach (°C)	5.5
<b>Condenser</b>	
Pressure (bar)	0.08
<b>Condenser pump</b>	
Isentropic efficiency (%)	75
Electro-mechanical efficiency (%)	98
<b>Feedwater pump</b>	
Isentropic efficiency (%)	78
Electro-mechanical efficiency (%)	98

Table 2: Nominal values of the Rankine cycle



190 2.3. *Thermal Energy Storage (TES)*

191 Thermal energy storage decouples energy production from solar hours  
192 and it allows a higher utilization of the power block since the extra heat  
193 produced by the solar field during the central hours can be exploited later  
194 during the day.

195 Different TES solutions have been evaluated for DSG, and one of the  
196 most promising is to split the system into different units depending on the  
197 water properties (Prieto et al., 2018): a preheater, an evaporator and super-  
198 heater unit. For this study, the proposed TES system uses a two concrete  
199 storage modules and a phase change material (PCM) unit. Compared to  
200 other sensible heat storage types such as molten salt tanks, in this study  
201 concrete storage has been selected because it is significantly less expensive  
202 (Lovegrove and Stein, 2012; Feldhoff et al., 2012; Prieto et al., 2018).

203 In figure 1 a scheme of the storage subsystem can be seen, sketched  
204 inside the dotted black box (**S**). The concrete storage units together with  
205 the PCM unit can be identified in the storage subsystem.

206 During the charging process, the heat from the superheated steam pro-  
207 duced in the solar field is extracted by the hot concrete unit using a heat  
208 exchanger integrated in the storage unit. At the exit of the hot concrete  
209 unit the saturated steam is introduced into the PCM that stores the latent  
210 energy from the steam as it condenses to water. The saturated water can  
211 be further cooled in the cold concrete unit. Then, the water can return to  
212 the solar field.

213 During the discharging process, the water coming from the power block  
214 is preheated in the cold concrete storage unit, evaporated in the PCM unit

215 and superheated up to 480 °C in the hot concrete storage unit. During  
216 the discharging process the steam pressure at the inlet of the power block  
217 falls to 95 bar and therefore the power block efficiency is reduced. During  
218 the operation using steam from the storage the cycle operates in sliding  
219 pressure mode.

220 To capture the heat losses of the storage subsystem a heat loss of 5 %  
221 (Montes et al. (2009a); Prieto et al. (2018)) has been assumed for this work.

#### 222 2.4. Design-point conditions

223 The design point of a solar power plant is commonly fixed at solar noon  
224 on the summer solstice (21st of June). The location of the solar power plant  
225 has been set at Seville, Spain. For this location the meteorological data  
226 (radiation, temperature and wind data) from the ASHRAE International  
227 Weather for Energy Calculations Version 1.1 (IWEC) has been used. The  
228 orientation of the receivers is North-South. Table 3 shows the design point  
229 conditions used for the calculations.

Parameter	Value
Collector orientation	N-S
Design point day	21 of June
Design Solar Time	12 h
Solar beam radiation (W/m <sup>2</sup> )	850
Ambient temperature (°C)	25
Location	Seville (Spain)
Latitude	37.42 °N
Longitude	-5.9 °E
Altitude (m)	31

Table 3: Design point conditions

230 At design conditions the optical efficiency of the Fresnel collectors,  $\eta_0$ ,  
231 is close to 0.65 (Novatec Solar (2017)). This parameter takes into account  
232 the receiver absorptivity, the mirrors (primary and secondary) reflectivity,  
233 the tracking errors and the fouling of mirrors and absorbers.

234 The incident thermal power of the field,  $\dot{Q}_{inc}$ , can be calculated as:

$$235 \quad \dot{Q}_{inc} = \eta_0 \cdot IAM \cdot A_{SF} \cdot DNI \quad (2)$$

236 where IAM is the incident angle modifier,  $A_{SF}$  is the total aperture area  
237 and DNI is the direct normal radiation. At design point the incident angle  
238 modifier has been considered one, otherwise, the incidence angle modifier  
239 can be calculated as the product of the traversal ( $K_t$ ) and longitudinal ( $K_l$ )  
240 correction factors (Mertins, 2008) (see section 2.5). The shadow losses and  
241 end losses (radiation reflected by the primary mirrors that does not reach  
242 the receiver) are neglected at design conditions.

243 The useful thermal output of the solar field is calculated as:

$$244 \quad \dot{Q}_{solar} = \dot{Q}_{inc} - \dot{Q}_{loss} - \dot{Q}_{pipes} \quad (3)$$

245 where  $\dot{Q}_{loss}$  and  $\dot{Q}_{pipes}$  are the heat losses in the solar field and pipes re-  
246 spectively.

247 To model the thermal loss of the solar receivers (PR70 Schott Advance)  
248 the experimental data from Burkholder and Kutscher (2008) has been used.  
249 The heat losses have been calculated using the following equation:

$$250 \quad \dot{Q}_{loss} = a_1(T_{ave} - T_{amb})^3 + a_2(T_{ave} - T_{amb})^2 + a_3(T_{ave} - T_{amb}) \quad (4)$$

251 where the coefficients  $a_1 = 6.779 \cdot 10^{-6}$  [W/K<sup>3</sup>],  $a_2 = -0.001823$  [W/K<sup>2</sup>],  
252  $a_3 = 0.3207$  [W/K] have been determined using the experimental data  
253 of PR70 Schott Advance at the National Renewable Energy Laboratory  
254 (NREL) (Burkholder and Kutscher, 2008).  $T_{ave}$  is the average temperature  
255 of the fluid in the solar field, (that is the average temperature of temper-  
256 ature at the exit of the last feedwater heater and at the inlet of the high  
257 pressure turbine) and  $T_{amb}$  is the ambient temperature (25 °C ).

258 The header pipes, that distribute the heat transfer fluid throughout the  
259 solar field, will also have an effect on the available heat of the Rankine  
260 cycle. To calculate the piping thermal losses of the solar field a constant  
261 value of  $q_{pipes} = 0.86$  W/m<sup>2</sup> has been employed. Therefore, these thermal  
262 losses depend on the solar field configuration.

### 263 2.5. *Off-design model*

264 The tracking system of the N-S linear Fresnel allows to track the sun  
265 to minimize the incidence solar angle on the collector surface. Neverthe-

266 less, there is an effect on the energy collected by the solar collector due to  
 267 the incidence angle. This effect is the incidence angle modifier, IAM. Fur-  
 268 thermore, under off-design conditions the performance of the solar field  
 269 might diminish due to the shading between solar collectors of different  
 270 rows. This effect is accounted on the shadowing efficiency,  $\eta_{shad}$ . Finally,  
 271 the factor that takes into account the losses due to the fact that part of the  
 272 radiation reflected by the mirrors does not reach the end of the receiver  
 273 is called end-loss efficiency,  $\eta_{end}$ . Equation 5 is used to obtain the thermal  
 274 energy collected by the solar field under off-design conditions:

$$275 \quad \dot{Q}_{inc,off} = \eta_0 \cdot IAM \cdot \eta_{end} \cdot \eta_{shad} \cdot A_{SF} \cdot DNI \quad (5)$$

276 As was stated above, the incidence angle modifier, IAM, can be calculated  
 277 as the product of the traversal,  $K_t$  and longitudinal factors,  $K_l$ . Equations  
 278 6 and 7 have been used to calculated them (Wagner, 2012).

$$279 \quad K_t = 0.9896 + 0.044 \cdot \theta_t - 0.0721 \cdot \theta_t^2 - 0.2327 \cdot \theta_t^3 \quad (6)$$

$$281 \quad K_l = 1.0031 - 0.2259 \cdot \theta_l + 0.5368 \cdot \theta_l^2 - 1.6434 \cdot \theta_l^3 + 0.722 \cdot \theta_l^4 \quad (7)$$

282 where  $\theta_t$  and  $\theta_l$  are the incidence traverse and longitudinal angles respec-  
 283 tively, that depend on the solar azimuth angle,  $\gamma$ , and the solar altitude  
 284 angle,  $\alpha$  (see eqs. 8 and 9) (Morin et al., 2012). Angles are expressed in *rad*.

$$285 \quad \theta_t = \tan^{-1} \frac{|\sin(\gamma)|}{\tan(\alpha)} \quad (8)$$

$$287 \quad \theta_l = \sin^{-1}(\cos(\gamma) \cdot \cos(\alpha)) \quad (9)$$

288 Figure 3 a shows the correction factors,  $K_t$  and  $K_l$ , with the incidence an-  
 289 gles, and figure 3 b shows the variation of the incidence angle modifier,

290 (IAM =  $K_t \cdot K_l$ ) with solar time for different days of the year (22 of March,  
 291 18 of June, 21 of September and 12 of December). Due to the North-South  
 292 orientation of the collectors the optical performance is slightly better in  
 293 mornings and evenings than on solar noon. This effect is more important  
 294 the further the day is separated from the summer solstice.

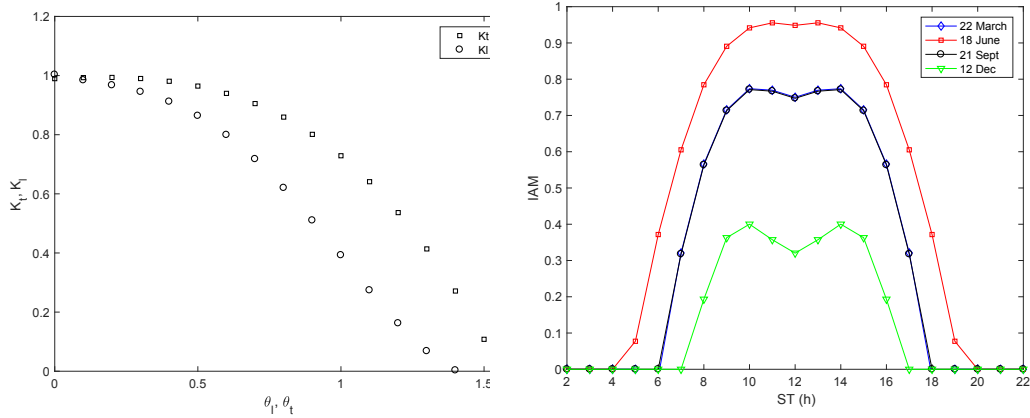


Figure 3: Optical performance of the Novatec Fresnel collector. a) Correction factors,  $K_t$  (square symbols) and  $K_l$  (circles), b) IAM for different days of the year at Seville.

295 It is necessary to take into account the part of the solar radiation re-  
 296 flected off the primary mirrors that is sent beyond the ends of the receiver  
 297 and secondary reflectors (Mertins, 2008). These losses,  $\eta_{end}$ , depend on the  
 298 longitudinal incidence angle,  $\theta_l$ , the receiver height,  $H_{rc}$  and the length of  
 299 the collector,  $L_{loop}$ .

$$300 \quad \eta_{end} = 1 - \frac{H_{rc}}{L_{loop}} \tan(\theta_l) = 1 - \frac{H_{rc}}{L_{cu} N_{cu}} \tan(\theta_l) \quad (10)$$

301 The position of the 16 mirrors of a control unit, together with the solar  
 302 incidence angle are used to determine the inclination of each mirror and  
 303 to calculate the shadowing. The two-dimensional model proposed by Pino

304 et al. (2013) has been used to calculate the inclination of the mirrors. This  
305 procedure is applied to every row and the total shaded area between rows  
306 is calculated. Finally, the shadow of the secondary reflector neighbour  
307 over the primary reflectors is taken into account. Eq. 11 describes the  
308 corresponding relation, where the shaded factor is this total shaded area,  
309  $A_{shad}$ , and  $A_{p_{cu}}$  is the reflective area of the control unit.

$$310 \quad \eta_{shad} = 1 - \frac{A_{shad}}{A_{p_{cu}}} \quad (11)$$

311 Finally, the hourly values of solar radiation of a "typical" year (from the  
312 ASHRAE International Weather for Energy Calculations),  $DNI$ , have been  
313 used to calculate the annual solar field energy.

#### 314 2.6. *Plant Performance at Partial Load*

315 The gross and net output of the plant are affected by the outlet con-  
316 ditions of the solar field (Lippke, 1995). The steam turbine operation at  
317 part load can be controlled by 3 methods: either by controlling the steam  
318 flow rate (throttle control and governing control) or adjusting the pressure  
319 (sliding pressure method) (Polsky, 1982). The *throttle control* method re-  
320 duces the steam mass flow rate by closing the "main steam stop valves",  
321 while the *governing control* regulates the steam flow rate by partially or to-  
322 tally closing sequentially the "steam control valves" that allow the steam  
323 into the arcs of the first stage of the high pressure turbine. Finally, in the  
324 *sliding-pressure* method (Spencer et al., 1963) the pressure at the inlet of the  
325 turbine is coupled with the pressure of the steam generator (no valves are  
326 closed) while the live steam temperature remains almost constant.

327 In this study, the steam turbine operation at part load is controlled by  
 328 the *sliding-pressure* method. To model the thermodynamic performance  
 329 of the Rankine cycle a Matlab code (Pérez-Cicala (2017)) has been used,  
 330 which models the power block performance off-design using the Stodola  
 331 law, as written by Patnode (2006):

$$332 \left( \frac{\dot{m}}{\dot{m}_{ref}} \right)^2 = \frac{P_1^2 - P_2^2}{P_{1,ref}^2 - P_{2,ref}^2} \quad (12)$$

333 where,  $P_{1,ref}^2 - P_{2,ref}^2$  is the pressure drop over a turbine section under de-  
 334 sign conditions and  $P_1^2 - P_2^2$  is the pressure drop over a turbine section at  
 335 partial load. Finally,  $\dot{m}$  and  $\dot{m}_{ref}$  are the mass flow rate of steam at partial  
 336 load and under design conditions, respectively. The turbine efficiency at  
 337 part load,  $\eta_T$ , as a function of throttle flow ratio (the ratio of mass flow rate  
 338 at part load to the mass flow rate at design conditions) has been calculated  
 339 using the method of Pérez-Cicala (2017).

340 Furthermore, the electro-mechanical efficiency of the generator at full  
 341 load is 98% (see table 2), and at partial load the efficiency of the electric  
 342 generator can be found using eq. 13 (Patnode, 2006).

$$343 \eta_{e,m} = 0.9 + 0.258 \cdot Load - 0.3 \cdot Load^2 + 0.12 \cdot Load^3 \quad (13)$$

344 where *Load* is calculated as the ratio between the turbine power and the  
 345 rated turbine power.

346 The gross power can be calculated:

$$347 \dot{W}_{gross} = \eta_{e,m} \cdot \eta_T \cdot \dot{Q}_{solar} \quad (14)$$

348 Finally, the net power from the cycle can be found out taking into account



349 the electric consumption of the solar field pumps, condenser pump, feed-  
350 water pump and the electrical consumption of the cooling water pump.

$$351 \quad \dot{W}_{net} = \dot{W}_{gross} - \dot{W}_{Parasitic} \quad (15)$$

### 352 **3. Cases studied**

353 Nine different solar field sizes and up to eight thermal storage sizes  
354 have been studied. The size of the solar field of the different cases studied  
355 can be seen in table 4. For each solar field the capacity of storage system  
356 has been varied from 0 hours to 8 hours.

357 The solar multiple,  $SM$ , has been used to characterize the solar lay-  
358 out (Schenk et al. (2014)). The  $SM$  is defined the ratio between the solar  
359 field thermal power,  $\dot{Q}_{solar}$ , at design conditions and the thermal power  
360 required by the power block,  $\dot{Q}_{PB,ref}$ , at nominal conditions (see eq. 16).  
361 In order to achieve the nominal conditions on the power block not only in-  
362 stantly, the solar multiple is always greater than one in solar plants (Montes  
363 et al. (2009b)).

$$364 \quad SM = \frac{\dot{Q}_{solar}}{\dot{Q}_{PB,ref}} \quad (16)$$

365 The thermal power required by the power block can be calculated as  
366 the ratio between the electrical power generated,  $\dot{W}_{gross}$  and the efficiency  
367 of the power block at full load.

$$368 \quad \dot{Q}_{PB,ref} = \frac{\dot{W}_{gross}}{\dot{\eta}_{T,ref} \eta_{e,m}} \quad (17)$$

369 Table 4 shows the simulation results for the solar field with different  
370 number of collector rows considered at the design point conditions for the  
371 DSG plant with no thermal storage.

Collector rows $N_{loops}$	Total Solar Field Area $A_{TOT} (m^2)$	Solar Field Aperture Area $A_{SF} (m^2)$	Solar Thermal Power $\dot{Q}_{solar} (MW_{th})$	Solar Multiple SM
32	$4.53 \cdot 10^5$	$2.47 \cdot 10^5$	130.54	1.03
38	$5.74 \cdot 10^5$	$3.12 \cdot 10^5$	165.36	1.31
44	$6.65 \cdot 10^5$	$3.62 \cdot 10^5$	191.47	1.51
50	$7.57 \cdot 10^5$	$4.11 \cdot 10^5$	217.57	1.72
58	$8.78 \cdot 10^5$	$4.77 \cdot 10^5$	252.39	1.99
64	$9.69 \cdot 10^5$	$5.26 \cdot 10^5$	278.50	2.20
72	$10.91 \cdot 10^5$	$5.92 \cdot 10^5$	313.31	2.47
80	$12.13 \cdot 10^5$	$6.57 \cdot 10^5$	348.12	2.75
88	$13.34 \cdot 10^5$	$7.23 \cdot 10^5$	382.93	3.02

Table 4: Summary of the simulation results at design conditions for solar plants of different solar field sizes with no storage.

## 372 4. Results and discussion

373 The thermal and optical model of the solar power plant operating un-  
374 der off-design conditions explained previously has been used to obtain the  
375 annual performance of the solar power plant with an hour timeframe.

### 376 4.1. Solar Field Performance

377 Figure 4 shows in combination with the DNI (right axis), the heat gen-  
378 erated by a solar field of 32 loops ( $SM = 1$ ) (right axis) on four representa-  
379 tive days of the year: March 21, June 18, September 21 and December 12,

380 using eq. 5. The days selected are clear days close to the equinoxes and  
381 solstices dates.

382 As could be expected, the thermal power is significantly higher on June  
383 18, especially if compared to the thermal power obtained on December 12,  
384 since the heat obtained in the solar field is related with the IAM (see eq. 5)  
385 and the IAM is maximum in the summer solstice.

386 The optical performance of the collectors during the day can be ob-  
387 served in figure 4 too. Despite the DNI is maximum at solar noon, the  
388 thermal power generated by the solar field at solar noon is slightly smaller  
389 than right before and after it because of the IAM reduction. **This effect is**  
390 **particularly important on December 12.**

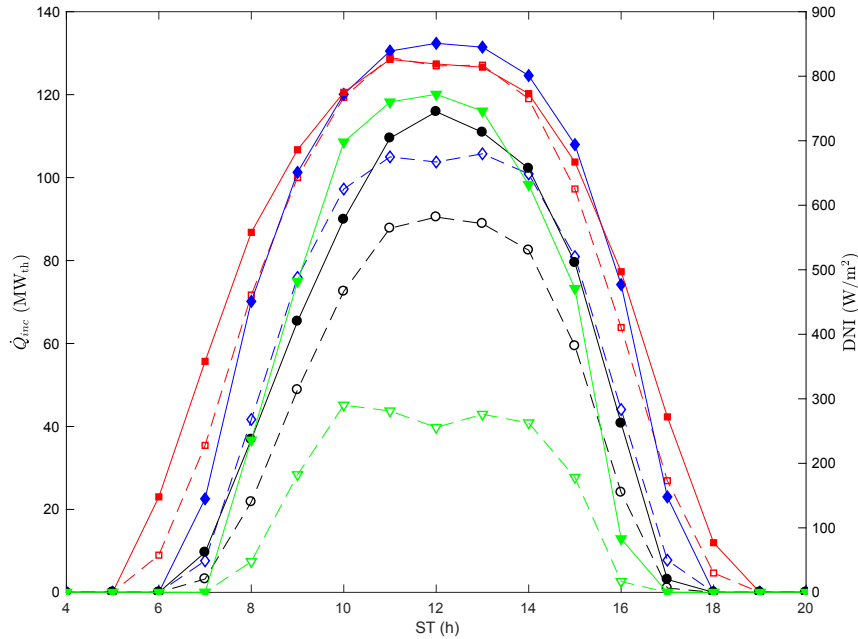


Figure 4: Direct solar radiation (right axis) and Thermal power generated (left axis) by the solar field on Mar 21 (blue  $\diamond$ ), June 18 (red  $\square$ ), Sept 21 (black  $\circ$ ) and 12 December (green  $\nabla$ ). Filled symbols correspond to DNI values and empty symbols to thermal power generated by the solar field.

#### 391 4.2. Annual electricity production

392 The capacity factor is the ratio of the net electricity generated, for the  
 393 time considered, to the energy that could have been generated at continu-  
 394 ous full-power operation during that period. For each solar field the max-  
 395 imum thermal storage has been calculated as the maximum thermal stor-  
 396 age that increased the capacity factor, i.e the maximum thermal storage  
 397 hours for the field of solar multiple of 1.99 is 6 hours, since a TES of 7  
 398 hours or bigger would give the same capacity factor of the plant.

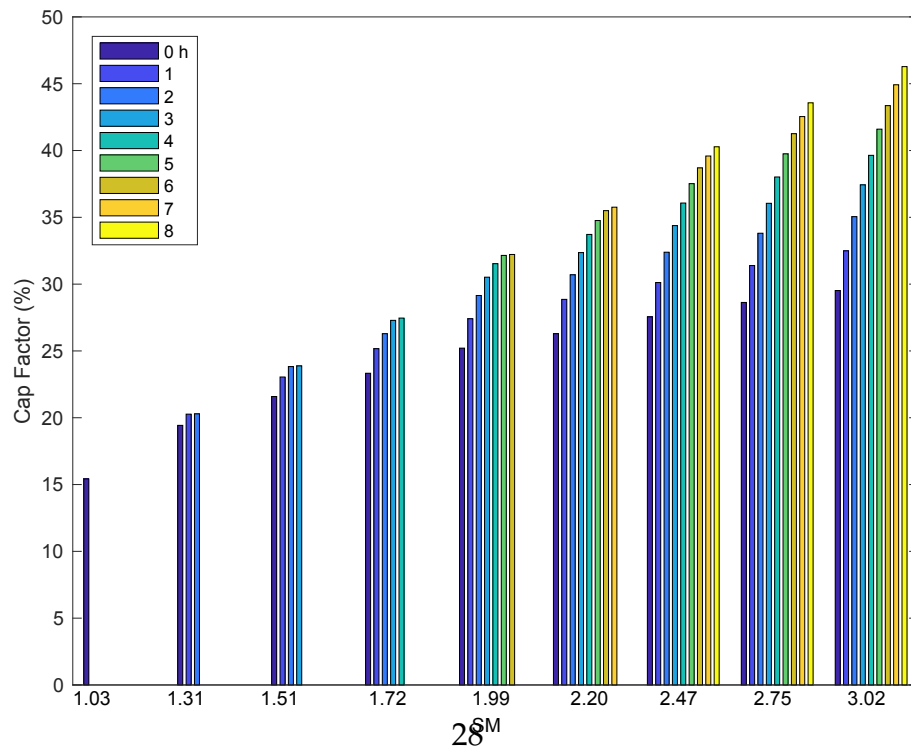
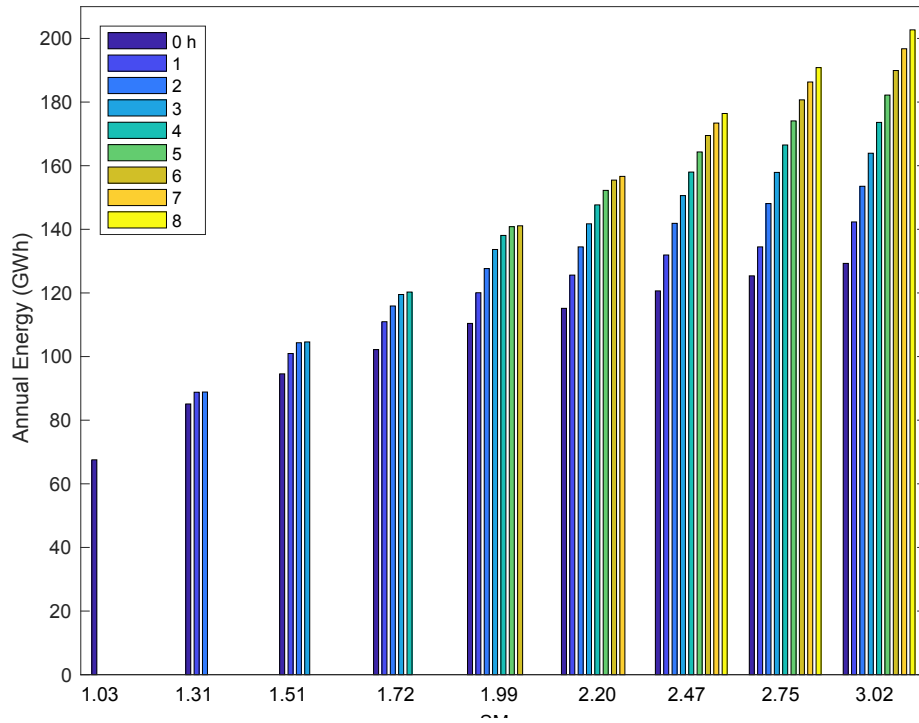


Figure 5: Summary of the annual results for different solar multiple (horizontal axis) and storage capacity (bar colors). a) Annual net electricity b) Capacity factor.

399 Figure 5 shows the annual electricity production (top figure) and ca-  
400 pacity factor (bottom figure) for different solar fields sizes and different  
401 thermal storage capacities. As was expected, the annual net electricity and  
402 capacity factor increase with the solar multiple. As the size of the solar  
403 field increases, so does the solar thermal power, and therefore the power  
404 block can operate longer producing more electricity. It is interesting to no-  
405 tice that the electricity yield (and hence, the capacity factor) increases non  
406 linearly with the solar multiple: it increases rapidly with the  $SM$  for small  
407 fields and more slowly with bigger fields. The explanation for this is that  
408 for a fixed storage capacity, increasing the solar field will initially make the  
409 steam turbine operate at full load for a longer period, but once the solar  
410 field is big enough, increasing even more the solar field will lead to mo-  
411 ments where the storage is full and the turbine is working at full load, and  
412 hence some of the solar thermal power produced will be unused.

413 It is **noteworthy** that, for the case of no thermal storage, the annual net  
414 electricity production is significantly smaller than for a parabolic trough  
415 solar plant. For the smallest solar field ( $SM = 1$ ), the annual net electric-  
416 ity yield of the plant with no storage is almost 60 % smaller than for a  
417 parabolic trough field of the same aperture area (Giotri et al. (2012)). This  
418 is due to the lower efficiency of the solar field of the LFR field compared  
419 to parabolic trough solar field.

420 The impact of the thermal storage in the capacity factor can be seen  
421 clearly in the solar plants with higher  $SM$ . It is not a linear relation: the  
422 impact of increasing the storage capacity is more important for lower stor-  
423 age capacities. The reason for this is that smaller storage capacities can be

424 exploited fully more days a year (days with clear sky and high irradiation)  
425 than bigger, which will be partially used in many occasions.

#### 426 4.3. Thermo-economic optimization

427 Based on the annual electricity production of the plants an economic  
428 study has been performed using different indicators: the Levelized Cost  
429 of Electricity and the Net Present Value.

430 The Levelized Cost of Electricity (LCOE, [ $\text{c}\text{€}/\text{kWh}_e$ ]) is one of the most  
431 important indicators to compare different power plants. It measures the  
432 total costs over the energy yield,  $E_{ann}$ . The value of the LCOE depends on  
433 the investment and operation and maintenance (O&M) costs,  $C_{O\&M}$ , that  
434 can vary depending of the country and the level of development of the  
435 technique.

436 The LCOE has been calculated using eq. 18.

$$437 \quad LCOE = \frac{C_{invest} \cdot (CRF + f_{ins,ann}) + C_{O\&M}}{E_{ann}} \quad (18)$$

438 where  $CRF$  is the capital recovery factor is defined as:

$$439 \quad CRF = \frac{i_{rate}(1 + i_{rate})^n}{(1 + i_{rate})^n - 1} \quad (19)$$

440 The annual insurance cost,  $f_{ins,ann}$ , the debt interest rate,  $i_{rate}$  and the  
441 detailed investment costs,  $C_{invest}$ , used to calculate the LCOE, are shown  
442 in the table below:

Parameter	Value
<b>Investment costs</b>	
Solar field cost ( $\text{€}/\text{m}^2$ )	120 <sup>1</sup>
Land cost ( $\text{€}/\text{m}^2$ )	2 <sup>2,3</sup>
Thermal storage cost ( $\text{€}/\text{kWh}_{th}$ )	65.65 <sup>4</sup>
Power block cost ( $\text{€}/\text{kW}_e$ )	700 <sup>3</sup>
Construction, engineering and contingencies (%)	20 <sup>3</sup>
—	—
Labour cost per employee and year ( $\text{€}/\text{year}$ )	48,000 <sup>5</sup>
Number of employees (for plant operation)	30 <sup>3</sup>
Number of employees (field maintenance), ( $\text{empl}/\text{m}^2$ )	$2 \cdot 10^{-5}$ <sup>5</sup>
O&M of investment per year (%)	1 <sup>2</sup>
—	—
Annual insurance cost, $f_{ins,ann}$ (%)	1 <sup>2,3</sup>
Lifetime (years), $n$	30 <sup>2</sup>
Debt interest rate, $i_{rate}$ (%)	8 <sup>2,3</sup>

Table 5: Cost data used the economical analysis. Sources: <sup>1</sup> Rovira et al. (2016). <sup>2</sup> Montes et al. (2009a). <sup>3</sup>Montes et al. (2009b). <sup>4</sup> Prieto et al. (2018) <sup>5</sup> Morin et al. (2012).

443 Figure 6 shows the LCOE for the different solar and storage sizes. Each  
444 solid line corresponds to the evolution of the LCOE with the solar multiple  
445 for a different storage capacity. The dashed black thick line corresponds to  
446 the minimum LCOE at each solar multiple (with different storage capaci-  
447 ties).



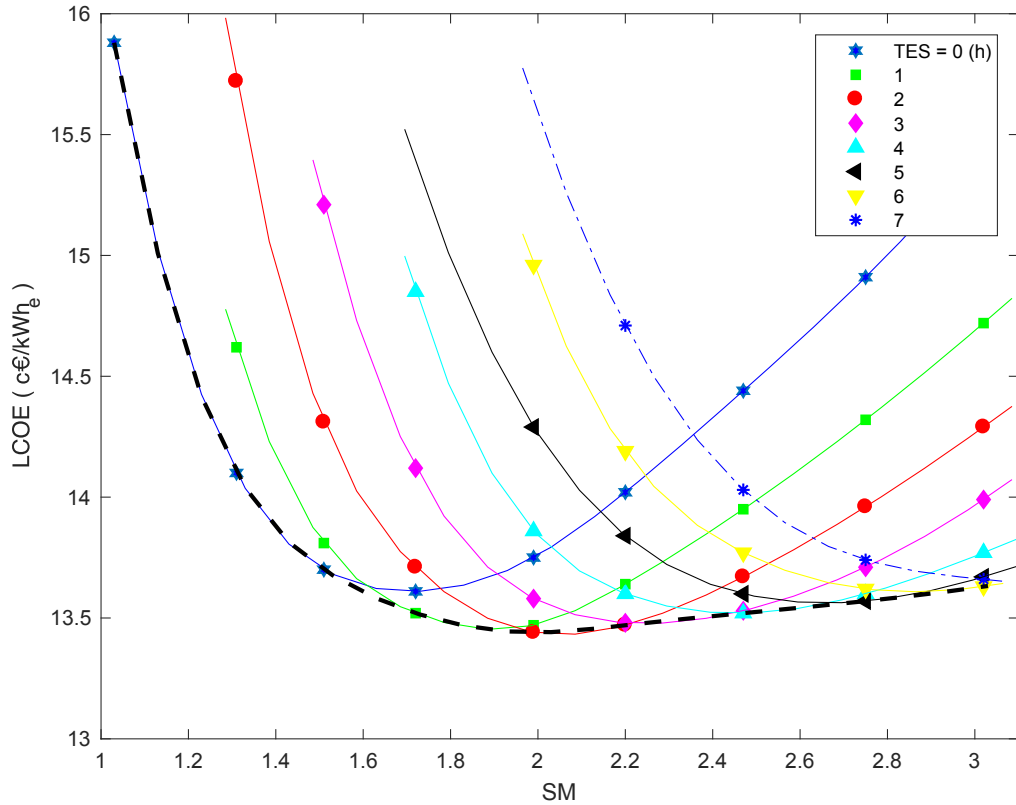


Figure 6: Influence of the storage size and solar multiple in the LCOE. Solid color lines represent power plants with different thermal storage capacity and dashed black thick line identifies the minimum LCOE of the Fresnel plants considered in the study.

448 For the case of no thermal storage (blue solid line with stars in fig. 6)  
 449 the LCOE presents a minimum, similarly to what happens in parabolic  
 450 plants (Montes et al. (2009b)). The LFR solar field has a lower efficiency  
 451 than the PTC solar field, but its costs is smaller, and hence the optimum  
 452  $SM$  is higher for the LFR. The optimum solar multiple in the case of LFR  
 453 technology is found at  $SM = 1.72$  with a value of  $13.61 \text{ c€/kWh}_e$ , whereas  
 454 Montes et al. (2009b) found the optimum  $SM$  for PTC plants was close to

455 1.2, and a LCOE of approximately 13.3 c€/kWh<sub>e</sub>.

456 It can be noticed, that for the cases of LFR plants with storage, the  
457 LCOE reaches a minimum, similar to the cases of no-storage. For each  
458 solar multiple, the optimum storage size that reduces the LCOE varies  
459 from 0 h (for the smallest solar field) to 5 hours (for the largest solar field).  
460 Furthermore, it can be seen for all the lines (all storage sizes), and espe-  
461 cially for the line representing the optimum plants (dashed black thick  
462 line), that the slope is bigger (in magnitude) for plants with  $SM$  smaller  
463 than the optimum than for solar plants with bigger  $SM$ . Hence, the so-  
464 lar field size plays a more important role for smaller LFR plants than for  
465 bigger ones, and increasing the solar field size over the optimum does not  
466 increase importantly the LCOE, whereas having a too small solar field in-  
467 creases notably the LCOE.

468 Regarding the thermal storage size, it can be seen that the higher is the  
469 solar multiple the larger is the thermal storage capacity that minimizes the  
470 LCOE. Or in other words, for LFR large solar field a high TES capacity is  
471 needed to ensure that the power block is working at full load during long  
472 periods of time and reduce the levelized cost of electricity. The optimum  
473 storage size (2 hours) is substantially smaller than when the heat transfer  
474 fluid is molten salts (15 hours according to Bacheller and Stieglitz (2017)),  
475 due to the high prices of the PCM storage compared with molten salts  
476 tanks.

477 It should be noted that the minimum LCOE is 13.44 c€/kWh<sub>e</sub>, corre-  
478 sponding to the case of  $SM = 1.99$  and 2 hours of TES.

479 On the other hand, the Total Net Present Value (TNPV) is a profit-based

480 indicator that allows to calculate the internal rate of return. This cost-  
481 benefit analysis is employed commonly when analyzing the profitability  
482 of CSP power plants (Li et al., 2014; Kost et al., 2013) or improvements  
483 implemented to these plants (Okoye and Atikol, 2014; Rodríguez-Sánchez  
484 et al., 2014; Marugán-Cruz et al., 2015). Naturally this analysis strongly  
485 depends on the cost assumptions and on the markets incentives for these  
486 plants.

487 The Spanish average market price from 2000 to 2017 (excluding 2008,  
488 which was an atypical year due to the high price of the barrel of Brent  
489 crude oil that almost reached the 150 \$ in June) is 4.16 c€/kWh<sub>e</sub> (OMIE,  
490 2017). The Spanish regulatory system, that was initially favorable to CSP  
491 development (BOE, 2007), has modified the remuneration scheme on sev-  
492 eral occasions increasing the investors risk. Under the current legislation,  
493 new renewable power plants will not receive any amount as remunera-  
494 tion on initial investment (BOE, 2014). This situation has led to no new  
495 installations of CSP plants in Spain since 2013. Due to the high investment  
496 costs, no CSP plant is cost competitive with traditional power plants and  
497 needs to be supported by feed-in tariffs or power-purchased agreements.  
498 However, for the calculation of TNPV, the average price of the remunera-  
499 tion for the current CSP plants in Spain since 2014 has been used: 29.557  
500 c€/kWh<sub>e</sub> (CNMC, 2017). The TNPV has been calculated using the follow-  
501 ing equation:

$$502 \quad TNPV = \sum_{k=1}^n \frac{B_k - C_k}{(1 + \tau)^k} \quad (20)$$

503 where  $B_k$  is the annual revenue,  $C_k$  represents the annual expenses,  $\tau$  is  
504 the discount rate (5.0%) and  $n$  is the service period (30 years). The rev-

505 enue is calculated as the Annual net Electricity (see figure 5) times the  
506 remuneration price (29.557 c€/kWh). The expenses are the operation and  
507 maintenance costs, the investment costs and repayment of the loans (see  
508 eq. 21).

$$509 \quad C_k = \left( IC - (k - 1) \frac{IC}{RY} \right) \cdot r + \frac{IC}{RY} \quad (21)$$

510 where  $IC$  is the total investment costs,  $r$  is the interest rate of the loans  
511 (8%),  $RY$  is the prepayment period of the loans (10 years). The costs are  
512 detailed in table 5.

513 The internal rate of return, IRR, has been calculated using eq. 20, as the  
514 discount rate that makes the TNPV zero at the end of the project. For all  
515 the plants the IRR is larger than 100%, and that is why the incentives im-  
516 plemented by the Spanish governments led to the installation of CSP. All  
517 configurations presented in this paper would be profitable in the scenario  
518 presented in the paper (remuneration of 29.557 c€/kWh<sub>e</sub>).

## 519 5. Conclusions

520 This paper presents a detailed analysis of the influence of solar field  
521 and energy storage size on the annual performance of direct steam gener-  
522 ation linear Fresnel plants with integrated thermal energy storage. In the  
523 present study, solar-only power plants have been considered (no fossil hy-  
524 bridation). A model for the off-design performance of the solar field has  
525 been developed to simulate the annual behaviour of a linear Fresnel power  
526 plant. The power block performance, both at nominal and part load, has  
527 been evaluated. **Based on the presented analysis the following conclusions**  
528 **have been drawn:**

- 529 • The size of the solar field (solar multiple) and the thermal storage  
530 capacity have been optimized to obtain the minimum LCOE, based  
531 on the annual performance simulations. The optimum LFR 50 MW<sub>e</sub>  
532 plant corresponds to a *SM* of 2 and TES of 2 hours with a LCOE of  
533 13.44 c€/kWh<sub>e</sub>. Despite of the lower efficiency of LFR, PTC and LFR  
534 plants present very similar values of LCOE.
- 535 • It has been found that increasing the solar multiple increases the en-  
536 ergy yield, and that its effect on the annual net electricity (and the  
537 capacity factor) of the LFR power plants is more important for small  
538 size solar fields. Compared to PTC plants using synthetic oil, which  
539 are the most common CSP plants, the optimum solar multiple is  
540 larger for DSG linear Fresnel plants because of the smaller efficiency  
541 of the linear Fresnel reflectors.
- 542 • The relation between the thermal storage capacity and the annual  
543 net electricity is non linear: as the TES size increases, so does the an-  
544 nual net electricity, and the effect of increasing the size of the thermal  
545 storage is more important on LFR power plants with small storage.
- 546 • DSG linear Fresnel plants with high storage capacity have higher  
547 capacity factor, but larger LCOE due to the high costs of TES systems  
548 for direct steam generation. Hence, the size of the TES has to be kept  
549 relatively small, since otherwise the LCOE increases importantly.

550 **Acknowledgements**

551 The authors gratefully acknowledge the financial support given by the  
552 Spanish Ministerio de Economía y Competitividad and the European Re-  
553 gional Development Fund through the project ENE2015-69486- R (MINECO  
554 /FEDER, UE). **The authors would like thank Felix Pérez-Cicala for his help**  
555 **with the partial-load code and his assistance with its modifications.**

556 **References**

- 557 Abbas, R., Muñoz, J., Martínez-Val, J. M., 2012. Steady-state thermal analy-  
558 sis of an innovative receiver for linear Fresnel reflectors. *Applied Energy*  
559 92, 503–515.
- 560 Al-Alili, A., Hwang, Y., Radermacher, R., 2012. A high efficiency solar air  
561 conditioner using concentrating photovoltaic/thermal collectors. *Ap-  
562 plied Energy* 93, 138–147.
- 563 Bacheller, C., Stieglitz, R., 2017. Design and optimisation of linear Fresnel  
564 power plants based on the direct molten salt concept. *Solar Energy* 152,  
565 171–192.
- 566 Barlev, D., Vidu, R., Stroeve, P., 2011. Innovation in concentrated solar  
567 power. *Solar Energy Materials and Solar Cells* 95, 2703–2725.
- 568 Bellos, E., Tzivanidis, C., Papadopoulos, A., 2018. Daily, monthly and  
569 yearly performance of a linear Fresnel reflector. *Solar Energy* 173, 517–  
570 529.

571 BOE, 2007. RD 661/2007. A22846-22886. Official State Gazette (in Spanish).  
572 <https://www.boe.es>, accessed: 2018-10-09.

573 BOE, 2014. RD 413/2014. BOE-A-2014-6123. Official State Gazette (in  
574 Spanish). <https://www.boe.es>, accessed: 2018-10-09.

575 Burkholder, F., Kutscher, C., 2008. Heat Loss Testing of Schott's 2008  
576 PTR70 Parabolic Trough Receiver. NREL Technical Report. NREL/TP-  
577 550-45633.

578 Cau, G., D., C., 2014. Use of parabolic trough solar collectors for solar re-  
579 frigeration and air-conditioning applications. Energy Procedia 45, 101-  
580 110.

581 CNMC, 2017. National Commission on Markets and Competition (in  
582 spanish). [https://www.cnmc.es/en/ambitos-de-actuacion/](https://www.cnmc.es/en/ambitos-de-actuacion/energia/liquidaciones-y-regimen-economico)  
583 [energia/liquidaciones-y-regimen-economico](https://www.cnmc.es/en/ambitos-de-actuacion/energia/liquidaciones-y-regimen-economico), accessed:  
584 2018-10-19.

585 Desai, N. B., Bandyopadhyay, S., 2017. Line-focusing concentrating solar  
586 collector-based power plants: a review. Clean Technology Environmen-  
587 tal Policy 19, 9-35.

588 Farjana, S. H., Huda, N., Parvez Mahmud, M., Saidur, R., 2018. Solar in-  
589 dustrial process heating systems in operation – Current SHIP plants and  
590 future prospects in Australia. Renewable and Sustainable Energy Re-  
591 views 91, 409-419.

592 Feldhoff, J. F., Benítez, D., Eck, M., Riffelmann, K. J., 2010. Economic  
593 potential of solar thermal power plants with direct steam generation

594 compared with HTF plants. *Journal of Solar Energy Engineering* 132,  
595 041001–1–9.

596 Feldhoff, J. F., Schmitz, K., Eck, M., Schnatbaum-Laumann, L., Laing, D.,  
597 Ortiz-Vives, F., Schulte-Fischedick, J., 2012. Comparative system analy-  
598 sis of direct steam generation and synthetic oil parabolic trough power  
599 plants with integrated thermal storage. *Solar Energy* 86, 520–530.

600 Gil, A., Medrano, M., I., M., Lázaro, A., Dolado, P., Zalba, B., Cabeza, L.,  
601 2010. State of the art on high temperature thermal energy storage for  
602 power generation. part 1-concepts, materials and modelization. *Renew-  
603 able and Sustainable Energy Reviews* 14, 31–55.

604 Giostri, A., Binotti, M., Astolfi, M., Silva, P., Macchi, E., Manzolini, G.,  
605 2012. Comparison of different solar plants based on parabolic trough  
606 technology. *Solar Energy* 86, 1208–1221.

607 González-Roubaud, E., Pérez-Osorio, D., Prieto, C., 2017. Review of com-  
608 mercial thermal energy storage in concentrated solar power plants:  
609 Steam vs. molten salts. *Renewable and Sustainable Energy Reviews* 80,  
610 133–148.

611 Grena, R., Tarquini, P., 2011. Solar linear Fresnel collector using molten salt  
612 nitrates as heat transfer fluid. *Energy* 36, 1048–1056.

613 Guo, J., Huai, X., Cheng, K., 2018. The comparative analysis on thermal  
614 storage systems for solar power with direct steam generation. *Renew-  
615 able Energy* 115, 217–225.



- 616 Guédez, R., Topel, M., Conde, I., F., F., Caballa, I., Spelling, J., Hassar, Z.,  
617 Pérez-Segarra, C., Laumer, B., 2016. A methodology for determining op-  
618 timum solar power tower plant configurations and operating strategies  
619 to maximize profits based on hourly electricity market prices and tariffs.  
620 *Journal of Solar Energy Engineering* 138, 021006–1–12.
- 621 Industrial Solar, 2017. Linear fresnel collector lf-11. [http://www.  
622 industrial-solar.de/en/products/fresnel-collector/](http://www.industrial-solar.de/en/products/fresnel-collector/),  
623 accessed: 2018-10-09.
- 624 Izquierdo, S., Montañés, C., Dopazo, C., Fueyo, N., 2010. Analysis of csp  
625 plants for the definition of energy policies: The influence on electric-  
626 ity cost of solar multiples, capacity factors and energy storage. *Energy*  
627 *Policy* 38, 6215–6221.
- 628 Johnson, M., Vogel, J., Hempel, M., Dengel, A., 2017. Design of high  
629 temperature thermal energy storage for high power levels. *Sustainable*  
630 *Cities and Society* 35, 758–763.
- 631 Johnson, M., Vogel, J., Hempel, M., Dengel, A., Seitz, M., Hachmann, B.,  
632 2015. High temperature latent heat thermal energy storage integration  
633 in a co-gen plant. *Energy Procedia* 73, 281–288.
- 634 Kolb, G. J., Clifford, H. K., Mancini, T. R., Gary, J. A., 2011. Power Tower  
635 Technology Roadmap and Cost Reduction Plan. Report No. SAND2011-  
636 2419, Albuquerque, NM, USA.
- 637 Kost, C., Flath, C. M., Möst, D., 2013. Concentrating solar power plant

- 638 investment and operation decisions under different price and support  
639 mechanisms. *Energy Policy* 61, 238–248.
- 640 Kumar, K. R., Reddy, K. S., 2012. 4-E (en-  
641 ergy–exergy–environmental–economic) analyses of line-focusing  
642 stand-alone concentrating solar power plants. *Int J Low-Carbon  
643 Technol* 7, 82–96.
- 644 Laing, D., Bauer, T., Breidenbach, N., Hachmann, B., Johnson, M., 2013.  
645 Development of high temperature phase-change-material storages. *Ap-  
646 plied Energy* 109, 497–504.
- 647 Laing, D., Eck, M., Hempel, M., Steinmann, W. D., Meyer-Grünefeldt, M.,  
648 Eickhoff, M., 2012. Analysis of operation test results of a high tempera-  
649 ture phase change storage for parabolic trough power plants with direct  
650 steam generation. In: *ASME 2012 6th Int. Conf. Energy Sustain. Parts A  
651 B. No. 273*.
- 652 Li, J., Wu, Z., Zeng, K., Flamant, G., Ding, A., J., W., 2017. Safety and effi-  
653 ciency assessment of a solar-aided coal-fired power plant. *Energy Con-  
654 version and Management* 150, 714–724.
- 655 Li, W., Wei, P., Zhou, X., 2014. A cost-benefit analysis of power genera-  
656 tion from commercial reinforced concrete solar chimney power plant.  
657 *Energy Conversion and Management* 79, 104–113.
- 658 Lippke, F., 1995. Simulation of the Part-Load Behaviour of a 30 MWe SEGS  
659 Plant. Report No. SAND95-1293, Albuquerque, NM, USA.

- 660 Lovegrove, K., Stein, W., 2012. Concentrating Solar Power Technology:  
661 Principles, Developments and Applications. Woodhead Publishing.
- 662 Luo, Y., Du, X., Yang, L., Xu, C., Amjad, M., 2017. Impacts of solar multiple  
663 on the performance of direct steam generation solar power tower plant  
664 with integrated thermal storage. *Frontiers in Energy* 11, 461–471.
- 665 Marugán-Cruz, C., Sánchez-Delgado, S., Rodríguez-Sánchez, M. R., M., V.,  
666 D., S., 2015. District cooling network connected to a solar power tower.  
667 *Applied Thermal Energy* 79, 178–2015.
- 668 Mertins, M., 2008. Technische und wirtschaftliche Analyse von horizontal  
669 en Fresnel-Kollektoren. PhD Thesis.
- 670 Mills, D., 2004. Advances in solar thermal electricity technology. *Solar En-  
671 ergy* 76, 19–31.
- 672 Mills, D., Morrison, G. L., 2000. Compact lineal Fresnel reflector solar ther-  
673 mal power plants. *Solar Energy* 68, 263–283.
- 674 Mokhtar, G., Boussad, B., Noureddine, S., 2016. A linear Fresnel reflector  
675 as a solar system for heating water: Theoretical and experimental study.  
676 *Case Studies in Thermal Engineering* 8, 176–186.
- 677 Mokhtar, M., Ali, M. T., Bräuniger, S., Afshari, A., Sgouridis, S., Arm-  
678 strong, P., M., C., 2010. Systematic comprehensive techno-economic as-  
679 sessment of solar cooling technologies using location-specific climate  
680 data. *Applied Energy* 87, 3766–3778.

- 681 Mokhtar, M., Berger, M., Zahler, C., Krüger, D., 2015. Direct steam gen-  
682 eration for process heat using Fresnel collectors. *Int. J. Therm. Eng.* 10,  
683 3–9.
- 684 Montes, M. J., Abánadez, A., Martínez-Val, 2009a. Performance of a direct  
685 steam generation solar thermal power plant as a function of the solar  
686 multiple. *Solar Energy* 83, 679–689.
- 687 Montes, M. J., Abánadez, A., Martínez-Val, J. M., Valdés, M., September  
688 2009b. Solar multiple optimization for a solar-only thermal power plant,  
689 using oil as heat transfer fluid in the parabolic trough collectors. *Solar*  
690 *Energy* 83, 2165–2176.
- 691 Morin, G., Dersch, J., Platzer, W., Eck, M., Häberle, A., 2012. Comparison  
692 of Linear Fresnel and Parabolic Trough Collector power plants. *Solar*  
693 *Energy* 86, 1–12.
- 694 Novatec Solar, 2017. Concentrated Solar Power by Novatec So-  
695 lar. [http://www.novatecsolar.com/40-1-Download-Centre.](http://www.novatecsolar.com/40-1-Download-Centre.html)  
696 [html](http://www.novatecsolar.com/40-1-Download-Centre.html), accessed: 2018-10-09.
- 697 NREL, 2018. Linear Fresnel Reflector Projects. [https://solarpaces.](https://solarpaces.nrel.gov/by-technology/linear-fresnel-reflector)  
698 [nrel.gov/by-technology/linear-fresnel-reflector](https://solarpaces.nrel.gov/by-technology/linear-fresnel-reflector), ac-  
699 cessed: 2018-10-09.
- 700 Okoye, C., Atikol, U., 2014. A parametric study on the feasibility of solar  
701 chimney power plants in North Cyprus conditions. *Energy Conversion*  
702 *and Management* 80, 178–187.

- 703 OMIE, 2017. Market Results. <https://www.omie.es>, accessed: 2018-10-  
704 09.
- 705 Patnode, A. M., 2006. Simulation and Performance Evaluation of Parabolic  
706 Trough Solar Power Plants. PhD Thesis.
- 707 Petrakopoulou, F., Sánchez-Delgado, S., Marugán-Cruz, C., Santana, D.,  
708 2017. Improving the efficiency of gas turbine systems with volumetric  
709 solar receivers. *Energy Conversion and Management* 149, 579–592.
- 710 Pino, F. J., Caro, R., Rosa, F., Guerra, J., 2013. Experimental validation of an  
711 optical and thermal model of a linear Fresnel collector system. *Applied  
712 Thermal Engineering* 50, 1463–1471.
- 713 Polsky, M. P., 1982. Sliding pressure operation in combined cycles. In: Pro-  
714 ceedings of the ASME. International Gas Turbine Conference and Ex-  
715 hibit. pp. 1–5.
- 716 Prieto, C., Rodríguez, A., Patiño, D., Cabeza, L. F., 2018. Thermal energy  
717 storage evaluation in direct steam generation plants. *Solar Energy* 159,  
718 501–509.
- 719 Pulido-Iparraguirre, D., Valenzuela, L., Serrano-Aguilera, J. J., Fernandez-  
720 Garcia, A., 2019. Optimized design of a Linear Fresnel reflector for solar  
721 process heat applications. *Renewable Energy* 131, 1089–1106.
- 722 Pérez-Cicala, J., 2017. Rankine cycle modelling using the Spencer, Cotton  
723 and Cannon Method (in Spanish). Masters Thesis.

- 724 Qiu, Y., He, Y.-L., Cheng, Z.-D., Wang, K., 2015. Study on optical and ther-  
725 mal performance of a linear Fresnel solar reflector using molten salt as  
726 HTF with MCRT and FVM methods. *Applied Energy* 146, 162–173.
- 727 Rodríguez-Sánchez, M. R., Sánchez-González, A., Marugán-Cruz, C., San-  
728 tana, D., 2014. Saving assessment using the PERS in solar power towers.  
729 *Energy Conversion and Management* 87, 810–819.
- 730 Rovira, A., Barbero, R., Montes, M. J., Abbas, R., Varela, F., 2016. Analy-  
731 sis and comparison of integrated solar combined cycles using parabolic  
732 troughs and linear Fresnel reflectors as concentrating systems. *Applied*  
733 *Energy* 162, 990–1000.
- 734 Schenk, H., Hirsch, T., Feldhoff, J. F., Wittmann, M., 2014. Energetic com-  
735 parison of linear Fresnel and parabolic trough. *Journal of Solar Energy*  
736 *Engineering* 136, 041015–1–041015–15.
- 737 Schott, 2017. Schott ptr70 receivers. the 4th gen-  
738 eration. [http://www.schott.com/d/csp/  
739 370a8801-3271-4b2a-a3e6-c0b5c78b01ae/1.0/schott\  
740 \\_ptr70\\\_4th\\\_generation\\\_brochure.pdf](http://www.schott.com/d/csp/370a8801-3271-4b2a-a3e6-c0b5c78b01ae/1.0/schott\_ptr70\_4th\_generation\_brochure.pdf), accessed: 2018-10-  
741 09.
- 742 Seitz, M., Johnson, M., Hibner, S., 2017. Economic impact of latent heat  
743 thermal energy storage systems within direct steam generating solar  
744 thermal power plants with parabolic troughs. *Energy Conversion and*  
745 *Management* 143, 286–294.

- 746 Singh, P., Sarviya, R. M., Bhagoria, J., 2010. Thermal performance of linear  
747 Fresnel reflecting solar concentrator with trapezoidal cavity absorbers.  
748 Applied Energy 87, 541–550.
- 749 Spencer, R. C., Cotton, K. C., N., C. C., 1963. A method for predicting per-  
750 formance of steam generators. 16,500 kw and larger. J. Eng. Power 4,  
751 249–298.
- 752 SUNCNIM, 2017. Fresnel Suncnim Solar Steam Generator. [https://www.suncnim.com/sites/default/files/2017-06/  
753 //www.suncnim.com/sites/default/files/2017-06/  
754 SUNCNIM\%20leaflet\%20EOR.pdf](https://www.suncnim.com/sites/default/files/2017-06/SUNCNIM\%20leaflet\%20EOR.pdf), accessed: 2018-10-09.
- 755 Velázquez, N., García-Valladares, O., Saucedo, D., Beltrán, R., 2010. Nu-  
756 merical simulation of a Linear Fresnel Reflector Concentrator used as  
757 direct generator in a Solar-GAX cycle. Energy Conversion and Manage-  
758 ment 51, 434–445.
- 759 Wagner, M. J., 2012. Results and Comparison from the SAM Linear Fresnel  
760 Technology Performance Model. NREL/CP-5500-54758 -.
- 761 Wagner, M. J., Zhu, G., 2012. A direct steam linear Fresnel performance  
762 model for NREL's System Advisory Model. In: Svartholm, N. (Ed.), Pro-  
763 ceedings of the ASME 2012 6th International Conference on Energy Sus-  
764 tainability and Fuel Cell Science, Engineering and Technology Confer-  
765 ence. pp. 1–8.
- 766 Wang, F., Zhao, J., Li, J., Deng, S., Yan, J., 2017. Preliminary experimental  
767 study of post-combustion carbon capture integrated with solar thermal  
768 collectors. Applied Energy 185, 1471–1480.

769 Yang, Y., Yan, Q., Zhai, R., Kouzani, A., Hu, E., 2011. An efficient way  
770 to use medium-or-low temperature solar heat for power generation e  
771 integration into conventional power plant. *Applied Thermal Energy* 31,  
772 157–162.

773 Zhu, G., Wendelin, T., Wagner, M. J., Kutscher, C., 2014. History, current  
774 state and future of linear Fresnel concentrating solar collectors. *Solar*  
775 *Energy* 103, 639–652.